Dynamics of Si−H−Si Bridges in Agostically Stabilized Silylium Ions

Samat Tussupbayev,[†] Georgii I. Nikonov,[‡] and Sergei F. Vyboishchikov*,[†]

Institut de Química Computacional, Campus de Montilivi, Universitat de Girona, 17071 Girona, Catalonia, Spain, and Chemistry Department, Brock University, 500 Glenridge Avenue, St. Catharines, Ontario L2S 3A1, Canada

Received: August 26, 2008; Revised Manuscript Received: November 10, 2008

The silylium ion $[C_6(SiMe_2)(SiHMe_2)_5]^+$ offers an amazing example of multiple Si···H interactions. It exhibits a symmetric $Si^{\alpha}-H-Si^{\alpha}$ motif supported by two additional $Si^{\beta}-H\cdots Si^{\alpha}$ agostic interactions. This cation is highly fluctional in NMR spectra at room temperature due to shift of the hydride bridge. The DFT calculations show that the hydride shift is related to internal rotation of silyl groups. We performed NMR, static DFT, and dynamics studies of this process and found two possible mechanisms, associated with internal rotation of either β- or γ-silyls. The energy barrier is largely caused by the silyl internal rotation, whereas the hydride transfer itself is intrinsically quite easy. The γ-silyl rotation is somewhat more favorable than the β-silyl rotation. Vibrational dynamics of the cation is also discussed.

Introduction

Three-coordinate silicon cations exhibit more electrophilic and more sterically accessible reaction centers than corresponding carbenium ions, which makes isolation of silylium ions very challenging.[1,2] The isolation of genuine three-coordinate silylium ions has been achieved only recently through the use of abundant steric protection and innocent counteranions.[3,4]

The intrinsic electrophilicity of silylium ions is so high that they easily react even with very weak nucleophiles.[5−11] To date, several cations stabilized by $(Si-H-Si)^+$,[12] $(Si-H-C)^+$,[13] $(Si-C-Si)^+$,[14] and $(Si-X-Si)^+$ [12b,15] (X = F, Cl, Br) bridges have been reported.[16] A related neutral B−H−Si system is also known.[17] Although most of these compounds are not fluxional, experimental data for the cation $[(Me_3Si)_3C(SiMePh)]^+$ suggest very facile alkyl and aryl scrambling between the silyl and the silylium positions.[14a]

Our interest in the dynamics of $(Si-H-Si)^+$ bridges was inspired by the report of Sakurai et al. that the hexa(fluorosilyl)benzene exhibits a "fluorine current" around the ring at elevated (328 K) temperatures (Chart 1).[18] Such dynamic behavior results in the splitting of the ^{29}Si signal due to the coupling to six equivalent fluorine nuclei. We reasoned that a hydrogen transfer in the related system $[C_6(SiHMe_2)_5(SiMe_2)]^+$ (**1**) would be an even easier process.

Here we report an NMR and DFT study of the dynamic behavior of the silylium ion **1**, underpinning the mechanism of hydride transfer in this system. A part of this work has already been communicated.[19]

Methods

NMR Method. NMR spectra were recorded on Bruker Avance AV600 spectrometer (^1H, 600 MHz) equipped with a BBO Z-grd ATM probehead in 5 mm tubes. ^1H NMR chemical shifts were referenced to residual protons of the solvent. Fluxional behavior was studied by low-temperature NMR and line-shape analysis.[20] Preparation of $[C_6(SiMe_2H)_5(SiMe_2)][B(C_6F_5)_4]$ was reported in the preliminary communication.[19]

CHART 1

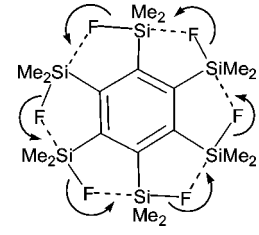

Computational Details

Static DFT Calculations. All geometry optimizations were carried out using the density-functional theory (DFT) with the Gaussian 03 program package,[21] applying the Perdew−Burke−Ernzerhof exchange and correlation functionals[22] (PBEPBE). An advanced GGA functional such as PBEPBE is a reasonable compromise between the quality and the computational costs. The standard 6-311G** basis set[23] was employed for geometry optimizations. No counterions were used. The nature of located stationary points was confirmed by the computation of harmonic force constants.

Molecular Dynamics Calculations. In this work, we have used molecular dynamics in two different forms. First, we employed the conventional Born−Oppenheimer molecular dynamics to simulate the vibrational behavior and obtain vibrational spectra of cation **1**. The Born−Oppenheimer dynamics simulations were performed using the CP2K code[24] at three different temperatures with a time step Δt of 1 fs. A low-temperature simulation (15 K) presumably should reproduce harmonic vibrational behavior, while higher-temperature runs (161 and 304 K) were performed to comprehend coupled large-amplitude vibrational motion.

To analyze the dynamics results, we used the velocity autocorrelation function, since the dipole moment could not be reliably obtained from calculations for technical reasons. The autocorrelation function $g(t)$ was evaluated at the kth time step using the standard equation as follows:

* Corresponding author. Fax: +34 97241 8356. Tel: +34 97241 8362. E-mail: vybo@stark.udg.es.
† Universitat de Girona.
‡ Brock University.

10.1021/jp807603t CCC: $40.75
Published on Web 01/21/2009

$$g(t_k) = \frac{N+1}{N-k+1} \frac{\sum_{m=0}^{N-k} v(t_{k+m})\, v(t_m)}{\sum_{m=0}^{N} v(t_m)\, v(t_m)} \qquad k = 0, \ldots, N$$

Here $N + 1$ is the total number of dynamics steps, and $v(t) = \dot{q}(t)$ was evaluated as a numerical derivative of a chosen internal coordinate q (a bond distance or a linear combination of bond distances) that is characteristic of the vibrational mode of interest. The choice of suitable internal coordinates will be given in the Results and Discussion section. The resulting vibrational spectral density $g(f)$ was obtained according to the formula:

$$g(1/n\Delta t) = \sum_{k=0}^{N} g(t_k)\, W(k) \exp\left(-\frac{2\pi i}{N+1} kn\right) \qquad n = 0, \ldots, N \quad (1)$$

with the Hamming windows function $W(t)$

$$W(k) = 0.53836 - 0.46164 \cos\left(2\pi \frac{k}{N-1}\right)$$

using the fast Fourier transform technique.

To better understand the coupling of vibrational modes in the dynamics, we also computed the correlation coefficient of various internal coordinates q, p to each other using the conventional formula known from the mathematical statistics as follows:

$$r(q,p) = \frac{n\sum_{k=0}^{N} q_k p_k - \sum_{k=0}^{N} q_k \cdot \sum_{k=0}^{N} p_k}{\sqrt{n\sum_{k=0}^{N} q_k^2 - (\sum_{k=0}^{N} q_k)^2} \cdot \sqrt{n\sum_{k=0}^{N} p_k^2 - (\sum_{k=0}^{N} p_k)^2}} \quad (2)$$

The electronic structure calculations were done using the PBEPBE functional as implemented in the Quickstep[25] module of CP2K. Quickstep is an implementation of the Gaussian Plane Wave (GPW) approach.[26] In this hybrid method, the Kohn−Sham molecular orbitals are described by linear combinations of Gaussian-type orbitals, whereas an auxiliary plane-wave basis set is employed to expand the electron density.[27] Double-ζ basis set[24,28] with polarization functions in conjunction with the Goedecker−Teter−Hutter pseudopotentials[29] (aliased as DZVP-GTH) were used. The auxiliary plane-wave basis set was defined by a cubic box of 16 × 16 × 16 Å^3 and by an energy cutoff of 300 Ry. The interaction between periodic images was canceled using an isolation technique.[30] To check the performance of the basis set chosen, we carried out geometry optimization of two different conformations of cation **1**. The conformation **1a** is the global minimum, while **1b** is higher in energy. The most important geometry parameters are given in Figure 1.

The comparison shows that bond distances resulting from the CP2K calculations are slightly larger (within 0.01 Å) than those from the Gaussian 03 calculation. The dihedral angles are virtually identical. The energy difference ΔE_e between **1a** and **1b** is 6.55 kcal·mol^{-1} and 6.51 kcal·mol^{-1} as calculated by Gaussian 03 and CP2K, respectively. This shows that the energetics and the geometry features obtained within the full-electron 6-311G** basis and by the double-ζ basis set within the GPW methods agree very well with each other.

Metadynamics Calculations. The metadynamics method allows for efficient sampling of the potential energy surface (PES) along one or several chosen internal coordinates (referred to as collective variables, CV). In this approach, a biasing potential is gradually constructed as a superposition of small Gaussian hills depending on the values of the CVs. The biasing potential effectively impels the system away from energy minima, thus facilitating sampling the areas of the transition states. The free energy profile as a function of the CVs, which is the main result of a metadynamics run, is then obtained from the accumulated biasing potential. In a converged metadynamics run, an arbitrary accuracy is achievable when using sufficiently small Gaussian hills.

It is important that the CVs clearly represent the process under study, since they determine the area of the PES to be sampled. In the present study, as the single CV we used the torsion angle C−C−Si−H that describes internal rotation of the corresponding silyl group about the C−Si bond. Two separate runs corresponding to the internal rotation of the β- and γ-silyl groups were performed. This choice of the CV will be clear from the Results and Discussion section.

After a series of test calculations, a Gaussian hill height was set to 0.25 kcal·mol^{-1} and the Gaussian width to 5°. The metadynamics step, that is, the time interval between hills, was chosen as 20 fs. The temperature was held within 300 K ± 50 K by rescaling atomic velocities.

Results and Discussion

NMR Studies. Cation **1** was prepared by hydride abstraction from $C_6(SiHMe_2)_6$ using $[Ph_3C][B(C_6F_5)_4]$ as previously described.[19] It was unambiguously characterized by IR and NMR spectroscopy, and the details of its structure were elucidated by means of DFT calculations.

At −80 °C, the ^{1}H NMR spectrum of **1** in CD_2Cl_2 exhibits three Si−H signals at 4.64 (γ-SiH), 4.41 (β-SiH), and 4.26 ppm (α-SiH), integrated as 2, 2, and 1 protons, respectively. They correspond to three Si−Me signals of equal intensity at 0.88 (α-SiMe), 0.67 (β-SiMe), and 0.48 ppm (γ-SiMe). The ^{29}Si NMR spectrum at −85 °C selectively decoupled from the methyl groups revealed three distinct signals with the ^{29}Si−^{1}H spin−spin coupling constants of 46.3 Hz, 118.9 Hz, and 170.7 Hz, for the α-, β-, and γ-Si atoms, respectively. These values indicate the presence of three types of Si−H protons. The lower coupling constant of 46.3 Hz establishes the presence of a Si−H−Si bridge, similar to what was observed in related systems.[12] The intermediate coupling constant (118.9 Hz) is significantly decreased compared with $HSiMe_2Ph$ (188.3 Hz), indicative of the presence of agostic $Si^{\alpha}\cdots H^{\beta}-Si^{\beta}$ interactions. Finally, the largest coupling constant of 170.7 Hz is nearly classical.

In the room-temperature ^{1}H NMR spectrum of **1**, the three Si−H signals merge into a single resonance integrated as 5 protons and the Si−Me signals merge into one singlet integrated as 36 protons, indicating a fluxional process due to a very facile shift of the silylium center throughout the ring. The room-temperature Si−H signal is flanked with ^{29}Si satellites which allow for the measurement of a very small average ^{29}Si−^{1}H coupling constant (23.0 Hz). Even more surprisingly, these satellites integrate to 25% of the overall intensity! As shown below, such a surprisingly small value of the *apparent Si−H coupling constant* is a direct result of low natural abundance of the ^{29}Si isotope (4.67%). Indeed, in a hypothetical all-^{29}Si isotopomer of **1** the room temperature Si−H coupling averaged over five protons could be estimated as (1/5)(2 × 46.3 Hz + 2 × 118.9 Hz + 2 × 170.7 Hz) = 134.4 Hz,[31] assuming that the ^{29}Si−^{1}H coupling constant does not alter much with temperature. However, because of low probability of finding more than one magnetically active silicon nucleus (^{29}Si isotope) in one

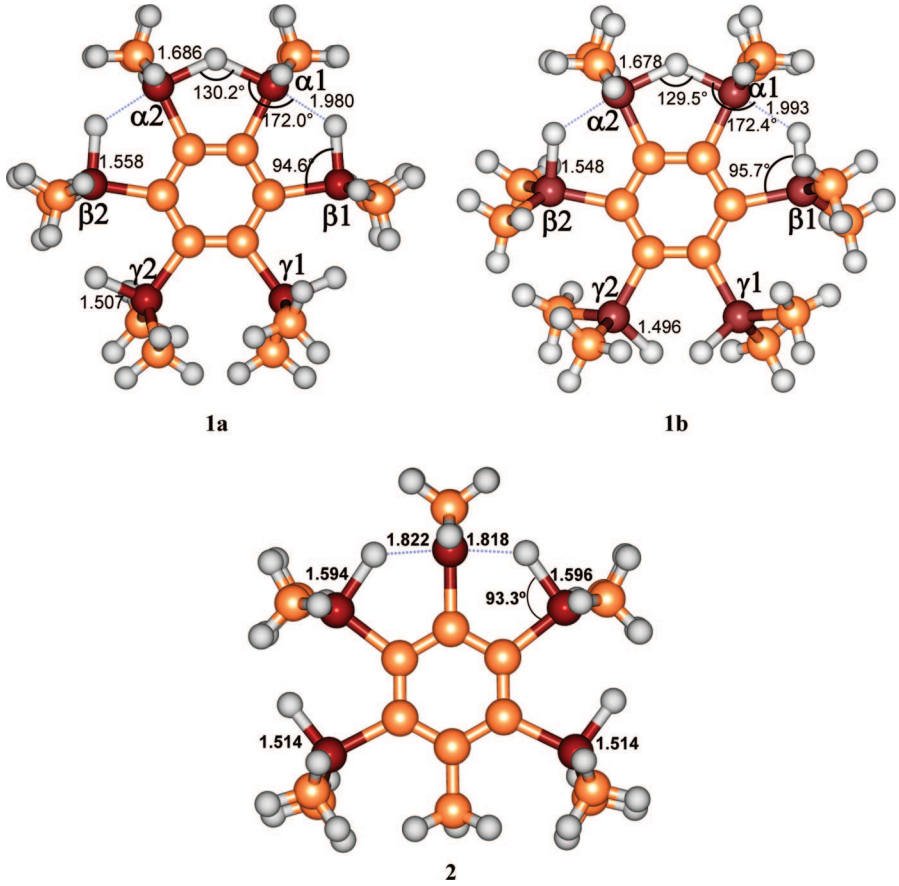

Figure 1. **1a** and **1b**: two rotamers of cation $[C_6(SiHMe_2)_5(SiMe_2)]^+$ and cation **2** $[1,4\text{-}C_6(SiMe_2)(Me)(SiHMe_2)_4]^+$.

molecule, the factor 1/6 should be applied.[32] The resulting coupling constant can be estimated as (1/6) × 134.4 Hz = 22.4 Hz, which is in good agreement with the experimental value of 23.0 Hz.

On the other hand, since there are six equivalent positions in the fluxional cation **1**, the probability of finding a molecule with the ^{29}Si nucleus in the NMR sample of **1** increases to 6 × 0.0467 = 0.2802, which again corresponds well to the experimentally observed increase of ^{29}Si satellites to 0.25. Further supporting this description is the observation of a second, much weaker set of satellites corresponding to J(H−Si) = 45.8 Hz (≈2 × 23 Hz). These satellites, stemming from the presence of two ^{29}Si isotopes in one molecule, have an intensity 3.2%, corresponding to the probability of finding two such nuclei in one molecule ({6 × 5/2} × 0.0467 × 0.0467 = 0.0327).[33]

Variable-temperature studies revealed the presence of two exchange processes. At about 215 K, the ^{1}H NMR signal for $SiMe^{\beta}$ group coalesces with the $SiMe^{\alpha}$ and $SiMe^{\gamma}$ signals. At about 213 K, the resulting two signals merge into one averaged signal. By applying the formula for two-site exchange, the upper limit for the activation barrier of the higher-energy process (exchange of α and γ positions) can be roughly estimated as $\Delta G^{\ddagger} = 10$ kcal·mol^{-1}.

DFT calculations of cation **1** (Figure 1) established a C_2 geometry with a symmetric Si−H−Si bridge between two α-Si centers. The $Si^{\alpha}-H^{\alpha}$ bonds (1.686 Å) are elongated compared to values observed in hydrosilanes (1.4−1.5 Å). A similar motif has been previously calculated for related Si−H−Si bridged silylium ions.[12] This α-Si−H−Si bridge is supported by two additional agostic $Si^{\alpha}\cdots H^{\beta}$ interactions, which contribute to the electronic saturation of the α-silicon atoms. The $Si^{\beta}-H^{\beta}$ bonds are also elongated (1.558 Å), albeit to a lesser extent than the $Si^{\alpha}-H^{\alpha}$ bonds, due to partial electron density transfer to the Si^{α} centers. The agostic $Si^{\alpha}\cdots H^{\beta}$ distance is stretched to 1.980 Å, which is comparable with distances observed in transition metal complexes with nonclassical Si−H interactions.[34] In contrast, the $Si^{\gamma}-H^{\gamma}$ bonds of 1.507 Å show no elongation compared to Me_3SiH. A $Si^{\beta}\cdots H^{\gamma}$ separation of 2.504 Å is too large for a significant interaction.

The ^{29}Si−^{1}H coupling constants were calculated as −38.2 Hz, −103.6 Hz, and −163.2 Hz for the α-, β-, and γ-Si centers, respectively.[19] Calculated ^{29}Si−^{1}H spin−spin coupling constants are generally very sensitive to molecular geometry. Since the calculated J(Si−H) values were in good agreement with the absolute experimental values discussed above, we concluded that the calculated molecular structure corresponds pretty well to the real one.

The formally analogous cation $[1,4\text{-}C_6(SiMe_2)(Me)(SiHMe_2)_4]^+$ (**2**) possesses a completely different structure (see Figure 1). It has a single silicon cationic center supported by two strong agostic Si−H bonds. Such a diagostic bonding is unprecedented in the silicon cation chemistry. Two $Si^{\beta}-H-Si^{\alpha}$ bridges are equivalent to each other but asymmetric with respect to the hydrogen position. The room-temperature ^{1}H NMR spectrum of **2** showed two Si−H signals, a septet at $\delta = 4.53$ for the γ-hydride, and a broad singlet at $\delta = 4.28$ for the β-hydride. The ^{29}Si NMR spectrum of **2** contained three signals. The α-silylium center gives rise to a multiplet at $\delta = 34.3$. Two β-silyls supporting the silylium ion via Si···H agostic interactions has a signal at $\delta = 33.5$ with a substantially weakened direct Si−H coupling ($^1J_{Si,H} = 87.2$ Hz, $^2J_{Si,H} = 6.9$ Hz). The γ-silyl exhibits a doublet of septets at $\delta = -4.5$ ($^1J_{Si,H} = 166.2$ Hz, $^2J_{Si,H} = 7.1$ Hz). The calculated values of the ^{29}Si−^{1}H spin−spin coupling constants[19] were found to be in good

agreement with the experiment. Contrary to cation **1**, the NMR spectral pattern of cation **2** does not change upon cooling down to −80 °C. This indicates the absence of fluxionality in this system.

Two important observations can be made from the comparison of cations **1** and **2**. First, the replacement of a $SiMe_2H$ group by a methyl strongly changes the coordination motif of the cationic fragment from a symmetric Si−H−Si bridge in **1** to the agostic coordination in **2**. The fact that such a strong structural change is caused by a rather small modification on a distant part of the molecule suggests that intrinsically the bridges are very labile. On the other hand, the lack of fluxionality in **2** suggests that the methyl acts as an "insulator", while the cation **1** presents a "conducting" medium with a relatively free motion of the cationic "hole" position. As such, the cation **1** can serve as a model for ionic conductors based on the Si−H chains. The above-mentioned NMR experiments demonstrate that cation **1** exhibits intriguing dynamics that deserves a special examination.

Static DFT calculations. Since our primary interest is the mechanism of the hydrogen migration in cation **1**, we first tried to locate various possible minima. The structure of one of the minima (**1a**) has already been reported in our preliminary communication.[19] Although the presence of four $SiMe_2H$ groups (β- and γ-), in principle, should provide a large conformational space, the agostic $Si^{\alpha}\cdots H^{\beta}$ bonds strongly restrain the internal rotation of the β-silyl groups. Such an internal rotation of the β-silyl groups would effectively destroy the agostic interaction, presumably destabilizing the cation. Still, their internal rotation cannot be completely ruled out, possibly contributing to the hydride transfer. On the other hand, the two γ-silyls do not seem to be important for the agostic support and could be expected to rotate, insofar as this is possible sterically.

In the structure **1a**, the cationic position ("hydride hole") is shared between two equivalent silicon atoms. This suggests that the dynamic behavior observed in the NMR spectra corresponds to a shift of the "hole" to another pair of silicon atoms. For instance, a Si−H−Si bridge could be formed between atoms denoted "α1" and "β1" in Figure 1. In this case, the formerly "α" and "γ" Si−H bond will turn agostic, still providing support for the bridge. The only essential difference with the original **1a** structure would be the position of the hydrogens themselves. An extensive search was performed to locate such a structure, but all attempts failed, the optimizations having resulted in the original **1a** geometry. We concluded that an additional motion is associated with the hydrogen transfer. This could be an internal rotation of a β- or γ-silyl group. It is possible that such a rotation itself causes the bridging hydrogens to migrate. In this case, the reaction coordinate for the migration process would be well represented by the corresponding dihedral angle, for example, C−C−Si−H. Thus, we now consider these two internal rotation processes.

***γ*-Silyl Rotation—Static DFT Study.** We performed a relaxed scan of the PES at various fixed values of the $C^{\beta 2}-C^{\gamma 2}-Si^{\gamma 2}-H^{\gamma 2}$ dihedral angle (hereafter denoted γ) varying from 0° to 180°. The resulting energy curve is given in Figure 2. The energy behaves rather parabolically in the vicinity of the **1a** minimum, which corresponds to γ of 15°. From γ of about 75° on, a rather flat transition state area begins, which spreads until γ of about 105°. Within this interval, the energy varies by less than 0.23 kcal·mol^{-1}. Thus, the exact position of the transition state is meaningless. We did a force-constant matrix analysis at several points in this interval to verify the correct (negative) curvature of the PES. Subsequently, the energy decreases rapidly and returns to the original value when

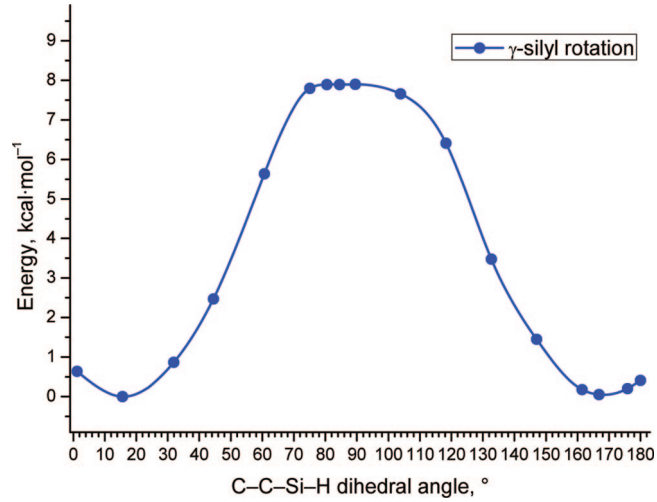

Figure 2. Relaxed scan of the PES of the cation **1a** with respect to the internal rotation of the γ-silyl group.

a half-rotation is completed. The energy barrier for the process, evaluated as the difference between the minimum energy and the highest energy along the curve, is 7.9 kcal·mol^{-1}.

We now consider the geometry changes in the course of the γ-silyl internal rotation process. The most interesting is the transition structure. In the transition geometry at $\gamma = 90°$ shown in Figure 3a, the cationic position is now clearly located at $Si^{\alpha 1}$. The formerly bridging $H^{\beta 1}$ is strongly shifted toward $Si^{\beta 1}$. Simultaneously, the $Si^{\alpha 2}-H^{\alpha}$ bond is elongated. All in all, this structure should be described as a silylium cation supported by two agostic bonds ($H^{\alpha}\cdots Si^{\alpha 1}$ and $H^{\beta 1}\cdots Si^{\alpha 1}$) rather than a bridged structure. It strongly resembles the equilibrium structure of cation **2** (see Figure 1), although the latter has approximate C_s symmetry. We see that the forced internal rotation of the γ-silyl by some 90° indeed causes the bridging hydride to move away from $Si^{\alpha 1}$ by about 0.2 Å. To better understand this process, we now consider the changes of other internal coordinates, notably the internal rotation angles and Si−H distances. They are summarized in Figure 4.

Figure 4a illustrates that the internal rotation of the γ-silyl group causes a significant variation of the β-silyl dihedral angle, which is not monotonic. The motion experienced by the β-silyl group is apparently a consequence of steric hindrance imposed by the changes in the position of the γ-methyls during the γ-silyl internal rotation. By doing this, the β-silyl adapts to the internal rotation of the γ-silyl. The largest deviation of the $C-C-Si^{\beta}-H^{\beta}$ dihedral angle from its original value occurs at about $\gamma = 60°$. Consequently, this forced β-silyl internal rotation results in a strong change in the $Si^{\alpha}\cdots H^{\beta}$ distance. Indeed, the Figure 4b shows that the $Si^{\alpha}\cdots H^{\beta}$ distance $r(Si^{\alpha 2}-H^{\beta 2})$ varies synchronously with the changes in the absolute value of the $C-C-Si^{\beta}-H^{\beta}$ dihedral angle. According to Figure 4b, $r(H^{\alpha}-Si^{\alpha 1})$ behaves antisymmetrically to $r(H^{\beta 1}-Si^{\alpha 1})$. While the γ-silyl rotates, they first reach an almost equal value at about $\gamma = 60°$. Subsequently they again go apart and cross again at γ about 120°. Finally $r(H^{\alpha}-Si^{\alpha 1})$ reaches the initial value of $r(H^{\beta 1}-Si^{\alpha 1})$, and vice versa. This means that the process of hydride bridge transfer is accomplished. This can be seen from the crossing point of the $r(H^{\beta 1}-Si^{\alpha 1})$ and $r(Si^{\beta 1}-H^{\beta 1})$ curves, which become bridging bonds, or from that of the $r(Si^{\beta 1}-H^{\gamma 1})$ and $r(H^{\alpha}-Si^{\alpha 2})$ curves, which become agostic bonds.

The above consideration shows that internal rotation of the γ-silyl indeed causes migration of the hydride bridge. Importantly, *no complete* internal rotation of the β-silyl takes place.

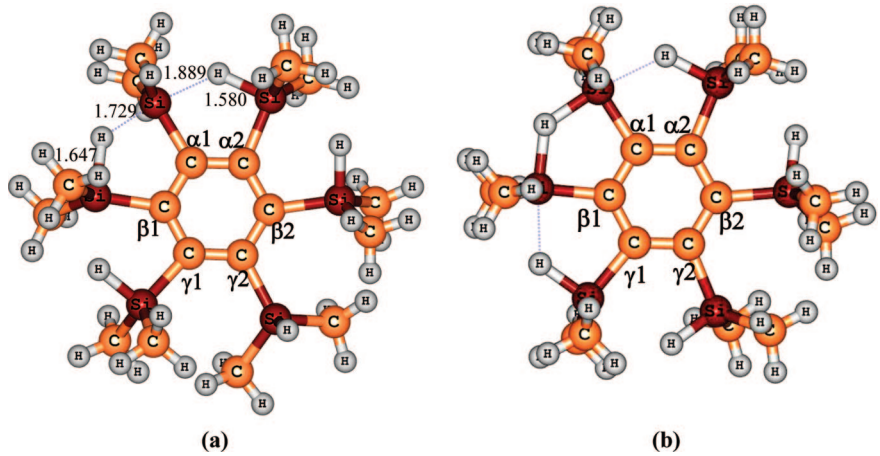

Figure 3. Transition structure obtained by internal rotation of the γ-silyl group in **1a** by 90° (a) and the final structure resulting from the rotation of the γ-silyl group by 180° is equivalent to **1a** (b).

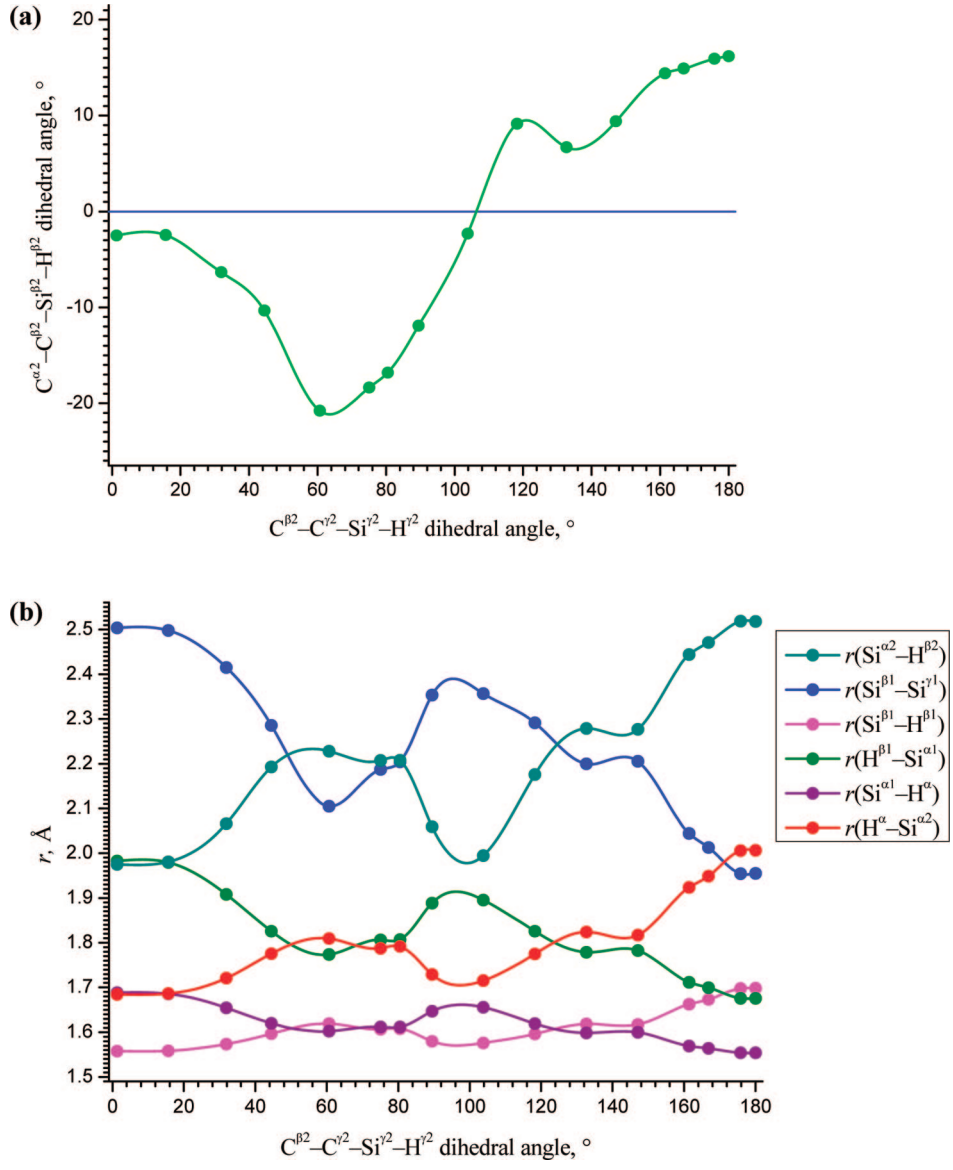

Figure 4. Changes in the C−C−Si$^{\beta}$−H$^{\beta}$ dihedral angle (a) and the Si−H distances caused by the internal rotation of the γ-silyl group (b).

Nonetheless, a small partial β-rotation induced by steric effects in the course of γ-rotation is sufficient to make the hydride transfer occur. The final structure resulting from the rotation of the Si$^{\gamma 2}$ group by 180° is equivalent to starting **1a**, with Si$^{\beta 1}$ being transferred to Si$^{\alpha 1}$ and Si$^{\gamma 1}$ being transferred to Si$^{\beta 1}$ (Figure 3b).

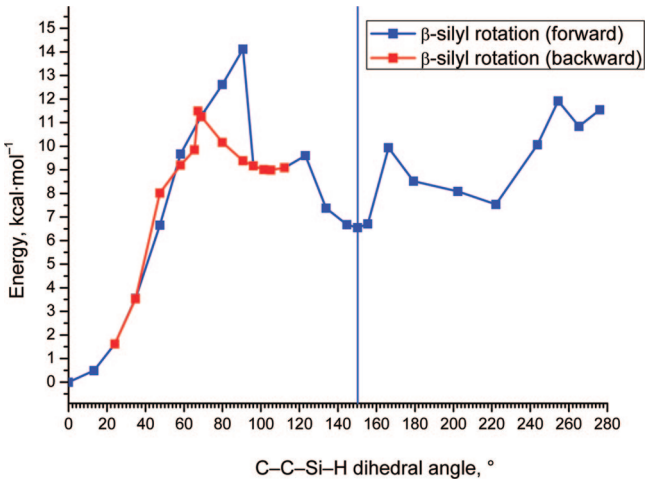

Figure 5. Relaxed scan of the PES of the cation **1a** with respect to the internal rotation of the β-silyl group. The double curve is a result of a hysteresis. The blue curve is obtained by the forward internal rotation of the β-silyl (increasing the $C^{\alpha}-C^{\beta}-Si^{\beta}-H^{\beta}$ dihedral angle). The red curve is obtained by the backward internal rotation going from 105° down to 0°.

***β*-Silyl Rotation—Static DFT Study.** The other possibility of initiating the hydride bridge transfer is to perform an internal rotation of the β-silyl directly. As we have seen, the complete rotation of the γ-silyl causes only a partial twisting of the β-silyl. Thus, if we force the β-silyl to make a full internal rotation, the pathway for the process should be different from that caused by γ-rotation. Therefore, we performed a relaxed PES scan along the $C^{\alpha}-C^{\beta}-Si-H$ dihedral angle β. The energy curve in the course of this process is reflected by Figure 5.

With increasing β from 0° on, the energy grows rapidly. The highest point with an energy of 14.1 kcal·mol^{-1} is achieved at $\beta \approx 90°$. However, no transition state could be located precisely. Then the energy drops sharply, and a local minimum is found at $\beta = 105.1°$ (see Figure 6a). This minimum, confirmed by an unconstrained geometry optimization with a subsequent force constant evaluation, is 9.0 kcal·mol^{-1} above the global minimum structure **1a**. Upon further rotation of the β-silyl, the system overcomes a small barrier at $\beta \approx 130°$ and reaches the minimum **1b** at $\beta = 150°$ (Figures 1b and 6b). This conformer **1b** is 6.6 kcal·mol^{-1} above the global minimum (8.1 kcal·mol^{-1} on the $\Delta G°_{298}$ scale).

The geometries of these two additional minima are very different (see Figure 6). The Si−H distances in the structure at $\beta = 105°$ (Figure 6a) strongly resemble that of the transition state for γ-silyl rotation (Figure 3a). That is, it features a single cationic silicon center supported by the donation from two neighboring Si−H bonds, albeit nonequivalent ones. In contrast, the conformer **1b** at $\beta = 150°$ (Figures 3b and 6b) has the exact C_2 symmetry and is very similar to the global minimum structure **1a**. They differ essentially in the orientation of two silyl groups opposite to the Si−H−Si bridge. In the 150°-structure, the Si−H bonds of the γ-silyl groups are directed toward each other, whereas in the global minimum **1a** they look in opposite directions. In the former, both $Si^{\gamma}-H$ are substantially out of plane, with the $C-C-Si^{\gamma}-H^{\gamma}$ dihedral angles of 28.9°. The elongated $Si^{\beta}-H$ bond also somewhat deviates from the plane, the $C-C-Si^{\beta}-H^{\beta}$ dihedral angles being 14.5°. For the global minimum **1a**, the γ- and β-dihedral angles are 15.7° and 2.5°, respectively.

As can be seen form Figure 6b, the Si−H−Si bridge in **1b** has already moved completely to a neighboring position. Due to the C_2 symmetry of **1b**, the $H^{\beta 2}$ and $H^{\gamma 2}$ atoms are equivalent, and the further process can go on equally by way of the $Si^{\beta 2}$ or $Si^{\gamma 2}$ internal rotation. In the former case, the system returns to the original **1a** configuration with increasing β dihedral angle. When rotating the $Si^{\gamma 2}$ silyl, also a **1a** structure emerges, but with the $Si^{\gamma 1}-H^{\gamma 1}-Si^{\beta 1}$ bridge. Thus, by this means the bridge shifts by two positions in total.

When performing the PES scan starting backward from the 105°-minimum, the resulting energy does not exactly coincide with the forward curve. The backward curve is shown in red in Figure 5. The potential energy initially increases gradually and rather harmonically from $\beta = 105°$ down to about 69°. Between about 90° and 60°, the energy is substantially lower than that of the forward scan. Thus, we observe a *hysteretic* behavior. At $\beta = 69°$, the backward curve crosses the forward one and then falls sharply and oscillates near the forward curve. This behavior is caused by an abrupt change in the conformation. From $\beta = 35°$ down, the backward and the forward curves coincide, and the structure returns to the original **1a** configuration. The highest energy point of the backward curve is reached at $\beta = 67°$ and is 11.5 kcal·mol^{-1} above the **1a** minimum. This is much lower than the forward-curve maximum of 14.1 kcal·mol^{-1}. Thus, in the course of the forward and backward scan, different conformations with very different energy are passed.

This hysteresis clearly indicates that the conformational space of cation **1** is rather complicated. There is no guarantee that we have actually passed through the lowest energy path when doing the relaxed PES scan. Although the highest energy point of 11.5 kcal·mol^{-1} may be a reasonable estimate of the ΔE energy barrier, a variety of paths occurring in reality may give rise to a quite different free energy profile than the ΔE curve from Figure 5. Nonetheless, the static DFT calculations indicate that both the β- and the γ-silyl rotation provide a plausible mechanism for the hydride transfer, the γ-rotation with a ΔE barrier of 7.9 kcal·mol^{-1} being more favorable.

Internal Rotation in the $C_6(SiHMe_2)_6$ Neutral System. Although our primary interest lies in the study of the $[C_6(SiMe_2)(SiHMe_2)_5]^+$ cation, a comparison with the corresponding neutral molecule can be useful to deeper understand the energetics of the cation. Since the $C_6(SiHMe_2)_6$ molecule has no bridging hydrogens, the energy barrier for the internal rotation of a dimethylsilyl group must be caused solely by steric effects.

To study the energetics of internal rotation of $C_6(SiHMe_2)_6$, we proceeded as follows. A hydrogen atom was added to the cationic **1a** structure. The resulting neutral system was optimized. As a consequence of steric hindrance, the benzene ring in the optimized structure is significantly nonplanar, with a sum of the six C−C−C−C dihedral angles of 93°. This helps the silyl groups to elude each other, but obviously costs some energy. Subsequently, a relaxed scan of the PES with respect to the C−C−Si−H dihedral angle of the γ-silyl group (relative to the former Si−H−Si bridge) was performed. In total, two different internal rotations in different directions (both counter- and clockwise) by 180° were followed. The resulting PES scan is depicted in Figure 7.

The counterclockwise rotation curve (the area of a positive abscissa in Figure 7) exhibits a single local maximum at about 115°, which is 9 kcal·mol^{-1} above the minimum. The benzene ring in the transition state is less distorted than in the minimum (the sum of the C−C−C−C dihedral angles is 52°), which means that the origin of the energy barrier is the direct repulsion between the silyl groups rather than the ring distortion energy.

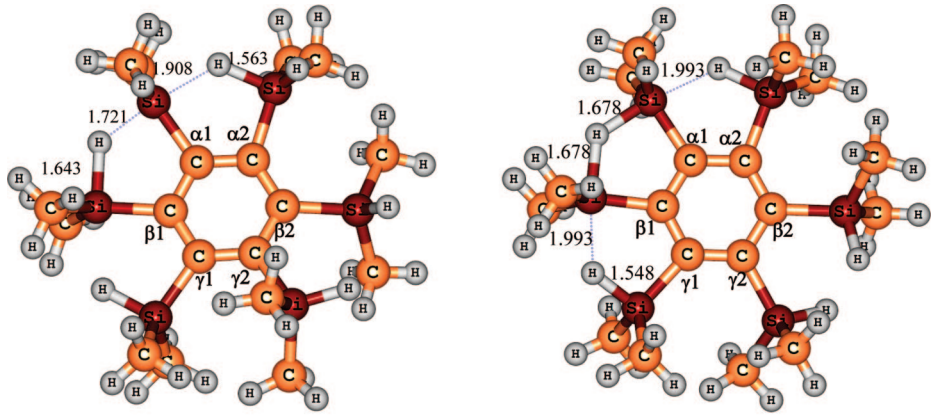

Figure 6. Additional minima obtained by internal rotation of the β-silyl group in **1a** by 105° (a) and by 150° (b; equivalent to **1b** from Figure 1).

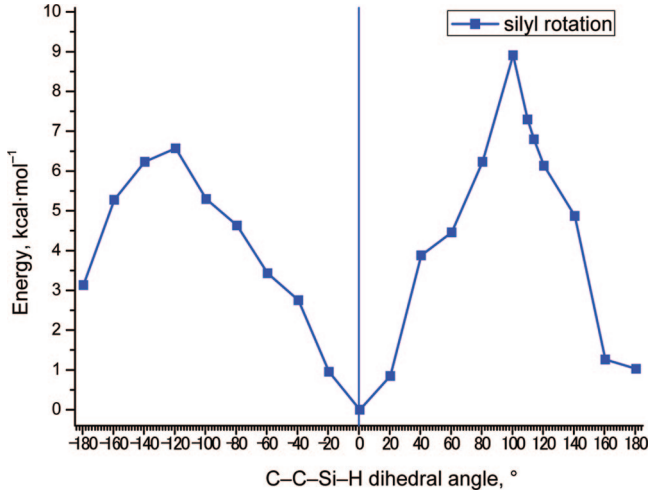

Figure 7. Relaxed scan of the PES of the neutral molecule $C_6(SiHMe_2)_6$ with respect to the internal rotation of a silyl group.

The clockwise-rotation curve (negative abscissa in Figure 7) behaves qualitatively similarly, but proceeds through a more favorable local maximum of 6.6 kcal·mol^{-1}. Importantly, the counter- and clockwise rotations by 180° result in *different* conformers that are 1.0 and 3.1 kcal·mol^{-1} above the starting minimum, respectively. This indicates that the actual conformational space of $C_6(SiHMe_2)_6$ may be much more complicated. Thus, the energy curves from Figure 7 do not necessarily represent the optimal ways of the silyl internal rotation. Nonetheless, we can take the values of about 9 kcal·mol^{-1} and 6.5 kcal·mol^{-1} as an estimate of the energy barrier caused by the steric bulk of the silyl group. Note that for the silyl internal rotation in the cation **1**, the corresponding barriers are about 11 and 8 kcal·mol^{-1}. We can roughly estimate the fraction of the barrier intrinsically caused by the hydride bridge motion to be about 2 kcal·mol^{-1}.

Vibrational Spectrum—Experiment and Harmonic Force-Constant Calculations. The experimental infrared spectrum of **1** exhibits bands at 1725 cm^{-1} and 1978 cm^{-1} (with a shoulder at about 1909 cm^{-1}) and a very broadband at about 2140 cm^{-1} (see Figure 8, Table 1). The analytical calculation of the harmonic vibrational frequencies for the structure **1a** yields a symmetric stretching vibration of two Si$^{\gamma}$−H bonds at 2134 cm^{-1}, their asymmetric vibration at 2131 cm^{-1} (with a much lower calculated intensity), the asymmetric and symmetric Si$^{\beta}$−H stretching at 1899 and 1898 cm^{-1}, respectively, and the asymmetric Si$^{\alpha}$−H−Si$^{\alpha}$ stretching vibration at 1655 cm^{-1}. The latter slightly underestimates the experimental value, but the two others are in excellent agreement with the experiment. While the γ-silyl stretching frequency lies in a region typical of hydrosilanes, the other two values exhibit a remarkable red shift of their Si−H bands, providing a strong evidence of weakened Si−H bonds in **1**. In fact, the Si$^{\alpha}$−H−Si$^{\alpha}$ bridge vibrational motion is coupled with the Si$^{\beta}$−H motions: stretching of one Si$^{\alpha}$−H bond is accompanied by stretching of the corresponding Si$^{\beta}$−H bond. The asymmetric Si$^{\beta}$−H vibration (1898 cm^{-1}) also contains an admixture of the Si$^{\alpha}$−H−Si$^{\alpha}$ stretching vibration.

Vibrational Spectrum from ab Initio Molecular Dynamics Simulations at 15 K. We calculated the vibrational frequency spectrum from the Fourier transform of relevant internal coordinates using eq 1. To facilitate the assignment of the resulting frequencies, we have chosen certain linear combinations (simple sums or differences) of Si−H interatomic distances. Thus, the internal coordinates used for the Fourier transform are as follows: $r(Si^{\alpha 2}-H^{\alpha}) - r(Si^{\alpha 1}-H^{\alpha})$, $r(Si^{\alpha 2}-H^{\alpha}) + r(Si^{\alpha 1}-H^{\alpha})$, $r(Si^{\beta 1}-H^{\beta 1}) - r(Si^{\beta 2}-H^{\beta 2})$, $r(Si^{\beta 1}-H^{\beta 1}) + r(Si^{\beta 2}-H^{\beta 2})$, $r(Si^{\gamma 1}-H^{\gamma 1}) - r(Si^{\gamma 2}-H^{\gamma 2})$, and $r(Si^{\gamma 1}-H^{\gamma 1}) + r(Si^{\gamma 2}-H^{\gamma 2})$, where $r(i-j)$ is the distance between the given atoms. They correspond, approximately, to the normal modes involving symmetric and asymmetric stretches of the Si−H bonds obtained in harmonic approximation. The graphs of the Fourier transforms are given in the Supporting Information, and the frequencies obtained are summarized in Table 1. By and large, the vibrational spectrum obtained from the vibrational dynamics at 15 K is rather similar to the analytical harmonic one, with some tendency of yielding slightly lower frequency values.

Statistical Analysis of the Vibrational Dynamics. To deeper understand how the motion of various atoms is coupled in the vibrational dynamics of cation **1**, we evaluated statistical data using the molecular dynamics trajectory. The most important of them are mean Si−H distances and their standard deviations given in Table 2.

Expectedly, all the Si−H average distances increase with temperature increasing from 15 to 161 K to 304 K. At 15 K the α-, β-, and γ-silyl distances are all clearly distinguishable within their respective standard deviations. However, at 161 K there is a slight overlap in the value of the Si$^{\alpha 1}$−H (1.724 Å ± 0.106 Å) and the Si$^{\beta 1}$−H distances (1.576 Å ± 0.053 Å), which

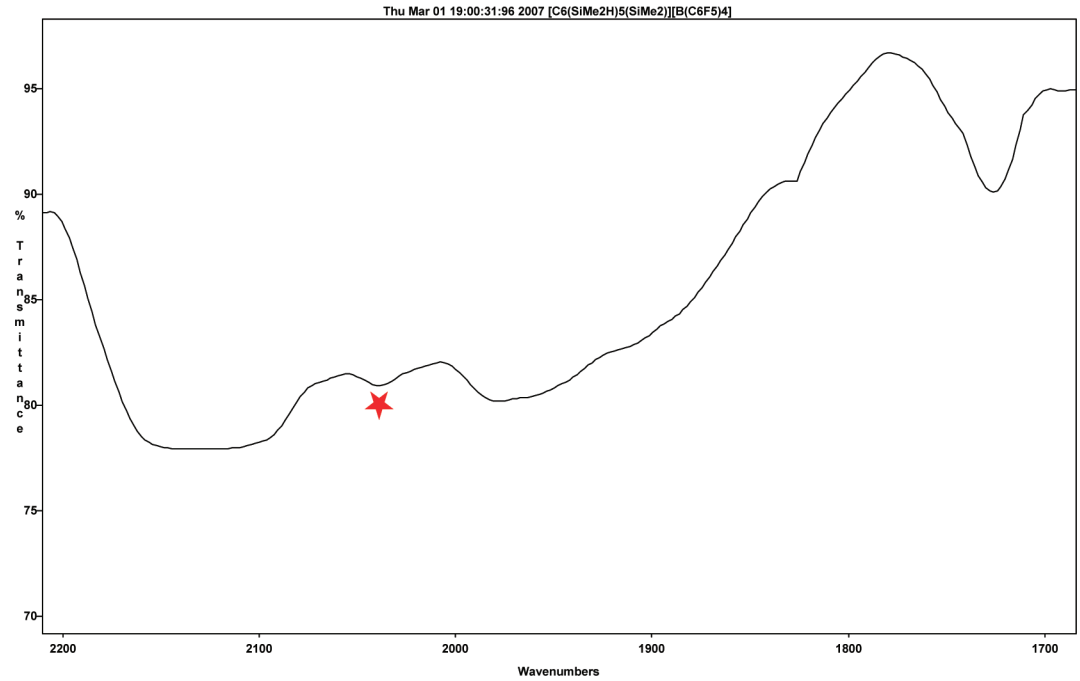

Figure 8. Infrared spectrum of **1** in Nujol. A weaker peak at 2030 cm^{-1} (marked with asterisk) comes from an impurity.

TABLE 1: Vibrational Frequencies of Si−H Bonds of the Cation 1a[a]

	DFT (harmonic)	molecular dynamics at 15 K	experiment
$Si^{\alpha}-H-Si^{\alpha}$	1655 (asym), 1248, 1213, and 1128 (sym)	1634 (asym), 1274, 1204, and 1137 (sym)	1725 (asym)
$Si-H^{\beta}$	1899 (asym), 1898 (sym)	1879 (asym), 1881 (sym)	1978, 1909 (shoulder)
$Si-H^{\gamma}$	2131 (asym), 2134 (sym)	2107 (asym), 2110 (sym)	2140 (broad)

[a] From the frequency spectrum of the corresponding internal coordinates.

TABLE 2: Mean Si−H Bond Distances $\langle r \rangle$ and Their Standard Deviations σ in Angstroms

	$\langle r \rangle$, Å			σ, Å		
	15 K	161 K	304 K	15 K	161 K	304 K
$Si^{\alpha 1}-H$	1.700	1.724	1.818	0.023	0.106	0.297
$Si^{\beta 1}-H$	1.565	1.576	1.604	0.010	0.053	0.106
$Si^{\gamma 1}-H$	1.513	1.518	1.525	0.005	0.029	0.035

becomes much larger at 304 K ($Si^{\alpha 1}-H$: 1.818 Å ± 0.297 Å; $Si^{\beta 1}-H$: 1.604 Å ± 0.106 Å).

A similar overlap occurs between the $Si^{\gamma 1}-H$ (1.518 Å ± 0.029 Å at 161 K; 1.525 Å ± 0.035 Å at 304 K) and $Si^{\beta 1}-H$ distances (1.576 Å ± 0.053 Å at 161 K; 1.604 Å ± 0.106 Å at 304 K). It follows that the $Si^{\alpha}-H$ bonds partly attain a character of $Si^{\beta}-H$ bonds (and vice versa), while $Si^{\beta}-H$ bonds slightly become of γ-silyl character. Interestingly, the dihedral angles γ and β vary in the range −62° to 62° and −36° to 36°, respectively. Thus, no full γ- or β-silyl internal rotation occurs on the time scale of the vibrational dynamics simulation. These results demonstrate that reversible hydrogen transfer occurs to some extent in the course of molecular vibration at 161 and 304 K without full γ- or β-silyl internal rotation. However, no scrambling (full mixing) of α-, β-, and γ-silyls takes place.

To get insight into coupling of vibrational coordinates in the course of dynamics, we computed the correlation coefficient of various internal coordinates to each other using eq (2; see Table 3). The strong coupling of both $Si^{\alpha}-H$ distances (a correlation coefficient of −0.7 or −0.6) obviously originates from the fact that stretching one of the $Si^{\alpha}-H^{\alpha}$ bonds is accompanied by a shortening of the other. The coupling between the bridged $Si^{\alpha}-H^{\alpha}$ bonds and the $Si^{\beta}-H^{\beta}$ bonds is also very strong (about 0.7). However, the coupling between the dihedral angle $C^{\alpha}-C^{\beta}-Si^{\beta}-H$ and the $Si^{\alpha}-H$ distance is very weak, with a correlation coefficient of −0.05. Thus, the shift of the central bridging α-hydride is accompanied by the change in the $Si^{\beta}-H$ distance, but not significantly by the β-silyl internal rotation. The correlation coefficients between the $Si^{\beta}-H$ and $Si^{\gamma}-H$ distances and between $Si^{\alpha}-H$ and $Si^{\gamma}-H$ bonds (about 0.25) are substantial, but much lower than that for the $Si^{\alpha}-H$ and the $Si^{\beta}-H$ bonds.

In principle, we can consider the hydrogen transfer process to have occurred if at a particular geometry configuration on the dynamics trajectory the α-bridge became less symmetric than the β-bridge. Quantitatively, this condition can be formulated as $|r(Si^{\alpha 2}-H^{\alpha}) - r(Si^{\alpha 1}-H^{\alpha})| > |r(Si^{\beta 1}-H^{\beta 1}) - r(Si^{\alpha 1}-H^{\beta 1})|$. It is interesting to see how frequently such configurations occur in the course of the dynamics. The statistics shows that at 15 K no such event occurs. In contrast, at 161 K the above condition is satisfied in 15% of cases and at 304 K in 30% of cases. If we formally consider this as a chemical process, its barrier can be evaluated as $\Delta G^{\circ} = -RT \ln K$, which yields $\Delta G^{\circ}_{161} = 0.55$ kcal·mol^{-1} if $K = 0.15$ and $T = 161$ K. For $K = 0.30$ and $T = 304$ K, we obtain $\Delta G^{\circ}_{304} = 0.51$ kcal·mol^{-1}. Therefore, we can take the value of 0.5 kcal·mol^{-1} as an estimate of intrinsic hydrogen transfer barrier, that is, that one not asociated with silyl internal rotation.

***γ*-Silyl Rotation—Metadynamics Simulations.** As can be seen from the static DFT calculations reported above, the reaction coordinate of the hydrogen transfer associated with the γ-silyl rotation is best represented by the dihedral angle $C^{\beta}-C^{\gamma}-Si^{\gamma}-H^{\gamma}$, which we denote γ. Therefore, we have chosen γ as the collective variable to study the γ-silyl rotation process.

TABLE 3: Correlation Coefficients of the Internal Coordinates *q* and *p*[a]

q	*p*	15 K	161 K	304 K
$d(Si^{\alpha 1}-H^{\alpha})$	$d(Si^{\alpha 2}-H^{\alpha})$	−0.703	−0.702	−0.581
$d(Si^{\alpha 1}-H^{\alpha})$	$d(Si^{\beta 1}-H^{\beta 1})$	0.701	0.666	0.739
$d(Si^{\beta 1}-H^{\beta 1})$	$d(Si^{\beta 2}-H^{\beta 2})$	−0.667	−0.413	−0.444
$d(Si^{\gamma 1}-H^{\gamma 1})$	$d(Si^{\gamma 2}-H^{\gamma 2})$	0.083	0.041	−0.158
$d(Si^{\beta 2}-H^{\beta 2})$	$d(Si^{\gamma 2}-H^{\gamma 2})$	0.309	0.249	0.580
$d(Si^{\alpha 2}-H^{\alpha})$	$d(Si^{\gamma 2}-H^{\gamma 2})$	0.276	0.260	0.553
$d(Si^{\alpha 2}-H^{\alpha})$	$d(C^{\alpha 1}-C^{\alpha 2})$	0.073	0.014	0.091
$a(H^{\beta 1}-Si^{\beta 1}-C^{\beta 1})$	$d(Si^{\alpha 1}-H^{\beta 1})$	0.406	0.542	0.677
$a(H^{\beta 1}-Si^{\beta 1}-C^{\beta 1})$	$d(Si^{\alpha 1}-H^{\alpha})$	−0.321	−0.409	−0.566
$a(H^{\beta 2}-Si^{\beta 2}-C^{\beta 2})$	$d(Si^{\alpha 2}-H^{\alpha})$	−0.277	−0.455	−0.554
$t(C^{\beta 2}-C^{\beta 2}-Si^{\beta 2}-H^{\beta 2})$	$d(Si^{\alpha 1}-H^{\alpha})$	0.113	0.097	0.194
$t(C^{\alpha 1}-C^{\beta 1}-Si^{\beta 1}-H^{\beta 1})$	$d(Si^{\alpha 1}-H^{\alpha})$	−0.049	−0.062	0.018
$t(C^{\beta 2}-C^{\gamma 2}-Si^{\gamma 2}-H^{\gamma 2})$	$t(C^{\alpha 2}-C^{\beta 2}-Si^{\beta 2}-H^{\beta 2})$	−0.140	0.026	0.029
$t(C^{\beta 2}-C^{\gamma 2}-Si^{\gamma 2}-H^{\gamma 2})$	$d(Si^{\alpha 2}-H^{\alpha})$	0.097	−0.085	−0.010
$t(C^{\beta 2}-C^{\gamma 2}-Si^{\gamma 2}-H^{\gamma 2})$	$t(C^{\beta 1}-C^{\gamma 1}-Si^{\gamma 1}-H^{\gamma 1})$	−0.083	−0.367	0.154
$t(C^{\alpha 2}-C^{\beta 2}-Si^{\beta 2}-H^{\beta 2})$	$t(C^{\alpha 1}-C^{\beta 1}-Si^{\beta 1}-H^{\beta 1})$	0.124	0.116	−0.012

[a] *d* are interatomic distances, *a* are angles, and *t* are dihedral angles.

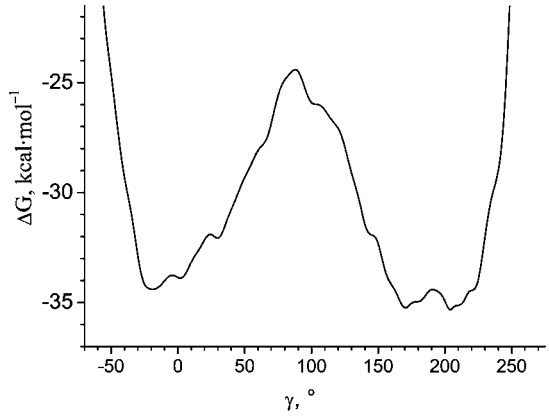

Figure 9. Free energy profile of the γ-silyl rotation from the metadynamics simulation.

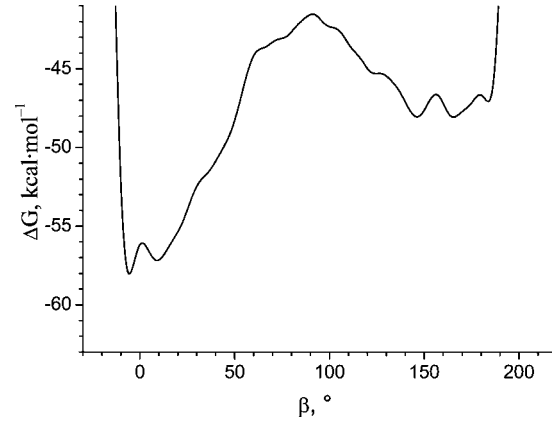

Figure 10. Free energy profile of the β-silyl rotation from the metadynamics simulation.

γ was allowed to vary from −60° to 250° by putting prohibitively high narrow Gaussian walls at these γ values. The free energy profile (2076 hills, 41532 fs) of the γ-silyl rotation obtained from the metadynamics simulation is shown in Figure 9. The shape of the resulting potential is close to a symmetrical double-well potential. The transition state area is approximately within γ of 75° to 108°, which is in good agreement with the static DFT results. The ΔG_{304} barrier of the γ-silyl rotation is about 10 kcal·mol^{-1}. This value is in a very close agreement with the static DFT result.

***β*-Silyl Rotation—Metadynamics Simulations.** The metadynamics simulation of the β-silyl rotation was performed using the dihedral angle $C^{\alpha}-C^{\beta}-Si^{\beta}-H^{\beta}$ (denoted as β) as the collective variable. It was allowed to vary within −15° and +190°. The free energy profile (2670 hills, 53400 fs) of the β-silyl rotation obtained from the metadynamics simulation is shown in Figure 10. The global minimum lies in the area of 0° to 10°, which is consistent with the static DFT calculations. Another minimum, which is 10 kcal·mol^{-1} higher in energy, is rather broad and located at β about 140° to 170°. The transition state is found at about $\beta = 90°$. The free energy barrier of the β-silyl rotation is about 16 kcal·mol^{-1}.

Thus, the metadynamics calculations confirm the existence of two mechanisms for the hydride transfer (by means of the γ- and β-silyl internal rotation). The γ-silyl rotation is more favorable than the β-silyl rotation, in accordance with the static DFT results presented above.

Conclusions

We have performed a detailed study of the dynamical behavior of the cation $[C_6(SiMe_2)(SiHMe_2)_5]^+$. First, variable-temperature NMR experiments indicate that there are two processes taking place, both resulting in a shift of the Si−H−Si bridge position. The higher of the respective ΔG barriers is roughly estimated to be about 10 kcal·mol^{-1}.

The DFT calculations show that these processes are only possible when an internal rotation of a silyl group occurs. Either a β- or γ-silyl group can rotate, giving rise to two different hydride transfer mechanisms. The general picture of the hydride transfer obtained from the calculations is as follows. Rotating a β-silyl group forces the $Si^{\alpha}-H^{\beta}$ distances to increase, which increases the electrophilicity of the corresponding α-silyl. The bridging H^{α} then moves toward the Si^{α}, which in turn makes the other α-silyl more electrophilic. As a consequence, the β-hydride moves too, turning to the bridging one. In the first mechanism, the complete shift of the bridging position occurs by a full 180° rotation of the β-silyl group. In the second mechanism, a full rotation of the γ-silyl group takes place, which due to steric effects causes some (but not complete) internal rotation of the β-silyl. Thus, two mechanisms with two different barriers can occur, which is in line with experiment. The static DFT calculations yield ΔE_e barriers of 7.9 kcal·mol^{-1} for γ-silyl rotation and about 11.5 kcal·mol^{-1} for β-silyl rotation, the latter value being in good accord with experimental estimates.

A more complete description of the hydride transfer process was obtained from a metadynamics study, with respective γ-

and β-rotation dihedral angles as collective variables. These calculation yield the γ-silyl and β-silyl rotation barriers of 10 and 16 kcal·mol^{-1}, respectively, in acceptable agreement with the static DFT results.

We also attempted to estimate what proportion of the barrier is due to silyl internal rotation (which is of steric nature) and what is due to hydride transfer. These estimates indicate that the intrinsic hydrogen transfer barrier is between 0.5 and 2.5 kcal·mol^{-1}, while the remaining part of the barrier is due to the steric effects.

The analytic harmonic frequency analysis as well as vibrational dynamics reveals a clear difference between α-, β-, and γ-vibrations. According to the vibrational dynamics results, the Si−H bond exhibits moderate anharmonicity. At 15 K the vibrations are rather localized, whereas at 161 and 304 K there is a substantial, though incomplete, mixing of Si−H bonds, such that the β-silyls partly get an α-bridge character and vice versa.

Thus, the $[C_6(SiMe_2)(SiHMe_2)_5]^+$ cation is a rather labile and fascinating dynamic system.

Acknowledgment. This work was supported by the Spanish Ministry of Education and Science (Ramón y Cajal Program, Grant CTQ2005-02698, and Grant PCI2005-A7-0167) and the Research Corporation. We thank Ms. Z. Lin and Mr. A. Khalimon for the preparation of $C_6(SiHMe_2)_6$ and Mr. R. Simionescu for assistance with NMR experiments.

Supporting Information Available: Calculated geometries and absolute energies of the molecules under study and calculated vibrational dynamics spectra of cation **1**. This material is available free of charge via the Internet at http://pubs.acs.org.

References and Notes

(1) Reviews:(a) Müller, T. *Adv. Organomet. Chem.* **2005**, *53*, 155–216. (b) Reed, C. A. *Acc. Chem. Res.* **1998**, *31*, 325–332. (c) Lambert, J. B.; Kania, L.; Zhang, S. *Chem. Rev.* **1995**, *95*, 1191. (d) Chojnowski, J.; Stanczyk, W. *Main Group Chem. News* **1993**, *93*, 1371. (e) Lickiss, P. D. *J. Chem. Soc., Dalton Trans.* **1992**, 1333. (f) Eaborn, C. *J. Organomet. Chem.* **1991**, *405*, 173. (g) Lambert, J. B.; Schulz, W. J., Jr. In *The Chemistry of Organic Silicon Compounds*; Patai, S., Rappoport, Z., Eds.; Wiley: Chichester, 1989; Part 2, p 1007.

(2) (a) Schleyer, P. v. R. *Science* **1997**, *275*, 39–40. (b) Gaspar, P. P. *Science* **2002**, *297*, 785–786.

(3) (a) Lambert, J. B.; Zhao, Y. *Angew. Chem.* **1997**, *109*, 389; *Angew. Chem., Int. Ed. Engl.* **1997**, *36*, 400. (b) Kim, K.-C.; Reed, C. A.; Elliott, D. W.; Mueller, L. J.; Tham, F.; Lin, L.; Lambert, J. B. *Science* **2002**, *297*, 825. (c) Müller, T.; Zhao, Y.; Lambert, J. B. *Organometallics* **1998**, *17*, 278. (d) Belzner, J. *Angew. Chem.* **1997**, *109*, 1331–1334; *Angew. Chem., Int. Ed. Engl.* **1997**, *36*, 1277−1280. (e) Kuppers, T.; Bernhardt, E.; Eujen, R.; Willner, H.; Lehmann, C. *Angew. Chem., Int. Ed.* **2007**, *46*, 6346–6349. (f) Duttwyler, S.; Do, Q.-Q.; Linden, A.; Baldridge, K. K.; Siegel, J. S. *Angew.Chem., Int. Ed.* **2008**, *47*, 1719–1722.

(4) For a two-coordinate cation see:(a) Driess, M.; Yao, S.; Brym, M.; van Wüllen, C. *Angew. Chem., Int. Ed.* **2006**, *45*, 6730–6733.

(5) (a) Lambert, J. B.; McConnell, J. A.; Schulz, W. J., Jr *J. Am. Chem. Soc.* **1986**, *108*, 2482–2484. (b) Lambert, J. B.; McConnell, J. A.; Schilf, W.; Schulz, W. J., Jr *J. Chem. Soc., Chem. Commun.* **1988**, 455–456. (c) Prakash, G. K. S.; Keyaniyan, S.; Aniszfeld, R.; Heiliger, L.; Olah, G. A.; Stevens, R. C.; Choi, H. K.; Bau, R. *J. Am. Chem. Soc.* **1987**, *109*, 5123–5126. (d) Xie, Z.; Liston, D. J.; Jelinek, T.; Mitro, V.; Bau, R.; Reed, C. A. *J. Chem. Soc., Chem. Commun.* **1993**, 384–386. (e) Kira, M.; Hino, T.; Sakurai, H. *Chem. Lett.* **1993**, 153–156. (f) Bahr, S. R.; Boudjouk, P. *J. Am. Chem. Soc.* **1993**, *115*, 4514–4519. (g) Cremer, D.; Olsson, L.; Ottosson, C.-H. *J. Mol. Struct. (THEOCHEM)* **1994**, *313*, 91–109.

(6) (a) Lambert, J. B.; Zhao, Y.; Zhang, S. M. *J. Phys. Org. Chem.* **2001**, *14*, 370. (b) Reed, C. A.; Xie, Z.; Bau, R.; Benesi, A. *Science* **1993**, *262*, 402. (c) Xie, Z.; Manning, J.; Reed, R. W.; Mathur, R.; Boyd, P. D. W.; Benesi, A.; Reed, C. A. *J. Am. Chem. Soc.* **1996**, *118*, 2922–2928. (d) Kira, M.; Hino, T.; Sakurai, H. *J. Am. Chem. Soc.* **1992**, *114*, 6697–6700.

(7) (a) Jutzi, P.; Bunte, A. E. *Angew. Chem., Int. Ed. Engl.* **1992**, *31*, 1605. (b) Steinberger, H.-U.; Müller, T.; Auner, N.; Maerker, C.; Schleyer, P. v. R *Angew. Chem., Int. Ed. Engl.* **1997**, *36*, 626. (c) Schuppan, J.; Herrschaft, B.; Müller, T. *Organometallic* **2001**, *20*, 4584–4592. (d) Müller, T.; Bauch, C.; Ostermeier, M.; Bolte, M.; Auner, N. *J. Am. Chem. Soc.* **2003**, *125*, 2158–2168.

(8) Müller, T.; Meyer, R.; Lennatz, D.; Siehl, H.-U. *Angew. Chem., Int. Ed. Engl.* **2000**, *39*, 3074.

(9) (a) Lambert, J. B.; Zhang, S.; Stern, C.; Huffman, J. C. *Science* **1993**, *260*, 1917. (b) Lambert, J. B.; Zhang, S. *Chem. Commun.* **1993**, 383. (c) Schleyer, P. v. R.; Buzek, P.; Müller, T.; Apeloig, Y.; Siehl, H.-U *Angew. Chem., Int. Ed. Engl.* **1993**, *32*, 1471. (d) Olsson, L.; Cremer, D. *Chem. Phys. Lett.* **1993**, *215*, 433. (e) Lambert, J. B.; Zhang, S. *Science* **1994**, *263*, 984. (f) Pauling, L. *Science* **1994**, *263*, 983. (g) Olah, G. A.; Rasul, G.; Buchholz, H. A.; Li, X.-Y.; Sandford, G.; Prakash, G. K. S. *Science* **1994**, *263*, 983. (h) Reed, C. A.; Xie, Z. *Science* **1994**, *263*, 985. (i) Olah, G. A.; Rasul, G.; Buchholz, H. A.; Li, X.-Y.; Prakash, G. K. S. *Bull. Soc. Chim. Fr.* **1995**, *132*, 569. (j) Arshadi, M.; Johnels, D.; Edlund, U.; Ottosson, C.-H.; Cremer, D. *J. Am. Chem. Soc.* **1996**, *118*, 5120. (k) Werner, K.; Meyer, R.; Müller, T. *Book of Abstract 34th Organosilicon Symposium*, White Plains, NY, 2001; p PS2−9. (l) Lickiss, P. D.; Masangane, P. C.; Sohal, W. *Book of Abstract 34th Organosilicon Symposium*; White Plains, NY, 2001; p, C-16.

(10) (a) Maerker, C.; Kapp, J.; Schleyer, P. v. R. In *Organosilicon Chemistry: From Molecules to Materials* Auner, N., Weis, J., Eds.; VCH: Weinheim, 1995; Vol. II, p 329. (b) Maerker, C.; Kapp, J.; Schleyer, P. v. R. In *The Chemistry of Organic Silicon Compounds*; Rappoport, Z., Apeloig, Y., Eds.; Wiley: Chichester, 1998; Vol. 2, pp 513−556. (c) Ottosson, C.-H.; Cremer, D. *Organometallics* **1996**, *15*, 5309. (d) Apeloig, Y.; Merin-Aharoni, O.; Danovich, D.; Ioffe, A.; Shaik, S. S. *Isr. J. Chem* **1993**, *33*, 387–402.

(11) For silylium ions stabilized by conjugation with multiple bonds see:(a) Ichinohe, M.; Igarashi, M.; Sanuki, K.; Sekiguchi, A. *J. Am. Chem. Soc.* **2005**, *127*, 9978. (b) Sekiguchi, A.; Matsuno, T.; Ichinohe, M. *J. Am. Chem. Soc.* **2000**, *122*, 11250.

(12) (a) Müller, T. *Angew. Chem.* **2001**, *113*, 3123–3126. (b) Panisch, R.; Bolte, M.; Müller, T. *J. Am. Chem. Soc.* **2006**, *128*, 9676–9682. (c) Hoffmann, S. P.; Kato, T.; Tham, F. S.; Reed, C. A. *Chem. Commun.* **2006**, 767–769.

(13) (a) Xie, Z.; Bau, R.; Benesi, A.; Reed, C. A. *Organometallics* **1995**, *14*, 3933. For a Si−H−C bridge in a neutral system see:(b) Dorsey, C. L.; Gabbaï, F. P. *Organometallics* **2008**, *27*, 3065–3069.

(14) (a) Choi, N.; Lickiss, P. D.; McPartlin, M.; Masangane, P. C.; Veneziani, G. L. *Chem. Commun.* **2005**, 6023–6025. (b) Meyer, R.; Werner, K.; Müller, T. *Chem.−Eur. J.* **2002**, *8*, 1163.

(15) Sekiguchi, A.; Muratami, A.; Fukaya, N.; Kabe, Y. *Chem. Lett.* **2004**, *33*, 530–531.

(16) For intermediacy of such species in silicon substitution reactions see:(a) Eaborn, C.; Happer, D. A. R.; Hopper, S. P.; Safa, K. D. *J. Organomet. Chem.* **1979**, *170*, C9. (b) Eaborn, C. *J. Chem. Soc., Dalton Trans.* **2001**, 3397.

(17) (a) Wrackmeyer, B.; Tok, O. L.; Bubnov, Y. N. *Angew. Chem., Int. Ed.* **1999**, *38*, 124–126. (b) Wrackmeyer, B.; Milius, W.; Tok, O. L. *Chem. Eur. J.* **2003**, *9*, 4732–4738.

(18) Ebata, K.; Inada, T.; Kabuto, C.; Sakurai, H. *J. Am. Chem. Soc.* **1994**, *116*, 3595–3596.

(19) Khalimon, A. Y.; Lin, Z.; Simionescu, R.; Vyboishchikov, S. F.; Nikonov, G. I. *Angew. Chem.* **2007**, *46*, 4530–4533.

(20) Fiebolin, H. *Basic One- and Two-Dimensional NMR Spectroscopy*; Wiley: Weinheim, 2005; Chapter 11.

(21) Frisch, M. J.; Trucks, G. W.; Schlegel, H. B.; Scuseria, G. E.; Robb, M. A.; Cheeseman, J. R.; Montgomery, J. A., Jr.; Vreven, T.; Kudin, K. N.; Burant, J. C.; Millam, J. M.; Iyengar, S. S.; Tomasi, J.; Barone, V.; Mennucci, B.; Cossi, M.; Scalmani, G.; Rega, N.; Petersson, G. A.; Nakatsuji, H.; Hada, M.; Ehara, M.; Toyota, K.; Fukuda, R.; Hasegawa, J.; Ishida, M.; Nakajima, T.; Honda, Y.; Kitao, O.; Nakai, H.; Klene, M.; Li, X.; Knox, J. E.; Hratchian, H. P.; Cross, J. B.; Bakken, V.; Adamo, C.; Jaramillo, J.; Gomperts, R.; Stratmann, R. E.; Yazyev, O.; Austin, A. J.; Cammi, R.; Pomelli, C.; Ochterski, J. W.; Ayala, P. Y.; Morokuma, K.; Voth, G. A.; Salvador, P.; Dannenberg, J. J.; Zakrzewski, V. G.; Dapprich, S.; Daniels, A. D.; Strain, M. C.; Farkas, O.; Malick, D. K.; Rabuck, A. D.; Raghavachari, K.; Foresman, J. B.; Ortiz, J. V.; Cui, Q.; Baboul, A. G.; Clifford, S.; Cioslowski, J.; Stefanov, B. B.; Liu, G.; Liashenko, A.; Piskorz, P.; Komaromi, I.; Martin, R. L.; Fox, D. J.; Keith, T.; Al-Laham, M. A.; Peng, C. Y.; Nanayakkara, A.; Challacombe, M.; Gill, P. M. W.; Johnson, B.; Chen, W.; Wong, M. W.; Gonzalez, C.; Pople, J. A. *Gaussian 03*, Revision D.01; Gaussian, Inc., Wallingford, CT, 2004.

(22) Perdew, J. P.; Burke, K.; Ernzerhof, M. *Phys. Rev. Lett.* **1996**, *77*, 3865.

(23) (a) Krishnan, R.; Binkley, J. S.; Seeger, R.; Pople, J. A. *J. Chem. Phys.* **1980**, *72*, 650. (b) Blaudeau, J.-P.; McGrath, M. P.; Curtiss, L. A.; Radom, L. *J. Chem. Phys.* **1997**, *107*, 5016.

(24) The CP2K developers group. http://cp2k.berlios.de, 2004.

(25) VandeVondele, J.; Krack, M.; Mohamed, F.; Parrinello, M.; Chassaing, T.; Hutter, J. *Comput. Phys. Commun.* **2005**, *167*, 103.

(26) Lippert, G.; Hutter, J.; Parrinello, M. *Mol. Phys.* **1997**, *92*, 477.

(27) Perdew, J. P.; Burke, K.; Ernzerhof, M. *Phys. Rev. Lett.* **1996**, *77*, 3865.

(28) Krack, M.; Parrinello M. In *High Performance Computing in Chemistry*; Grotendorst, J., Ed.; Research Centre Jülich: Jülich, Germany, 2004; NIC series; Vol. 25, pp 29−51.

(29) (a) Goedecker, S.; Teter, M.; Hutter, J. *Phys. Rev. B* **1996**, *54*, 1703. (b) Krack, M. *Theor. Chem. Acc.* **2005**, *114*, 145.

(30) Martyna, G. J.; Tuckerman, M. E. *J. Chem. Phys.* **1999**, *110*, 2810.

(31) The single α-proton contributes twice to the formula because in the ^{1}H NMR spectrum of the all-^{29}Si isotopomer of **1** its signal would appear as a triplet (neglecting the H−H coupling to the Me group), whereas other Si−H signals would be doublets.

(32) Only one of six silicon atoms in **1** would contribute to coupling with protons, and the average *J*(Si−H) should be reduced by a factor of 1/6. We thank R. Simionescu for the explanation of this spectral feature.

(33) Combinatorial formula has been applied.

(34) Nikonov, G. I. *Adv. Organomet. Chem.* **2005**, *53*, 217–309.

JP807603T